Location of Long Period events belo Kilauea using seismic amplitudes and precise relative relocation.

Jean Battaglia, Jean-Luc Got, P. Okubo

Location of long-period events below Kilauea Volcano using seismic amplitudes and accurate relative relocation

Jean Battaglia[1,2]
Center for the Study of Active Volcanoes, Hilo, Hawaii, USA

Jean-Luc Got
Laboratoire de Géophysique Interne et Tectonophysique, Université de Savoie, Le Bourget du Lac, France

Paul Okubo
U.S. Geological Survey, Hawaii Volcano Observatory, Hawaii National Park, Hawaii, USA

Received 24 March 2003; revised 8 September 2003; accepted 19 September 2003; published 5 December 2003.

[1] We present methods for improving the location of long-period (LP) events, deep and shallow, recorded below Kilauea Volcano by the permanent seismic network. LP events might be of particular interest to understanding eruptive processes as their source mechanism is assumed to directly involve fluid transport. However, it is usually difficult or impossible to locate their source using traditional arrival time methods because of emergent wave arrivals. At Kilauea, similar LP waveform signatures suggest the existence of LP multiplets. The waveform similarity suggests spatially close sources, while catalog solutions using arrival time estimates are widely scattered beneath Kilauea's summit caldera. In order to improve estimates of absolute LP location, we use the distribution of seismic amplitudes corrected for station site effects. The decay of the amplitude as a function of hypocentral distance is used for inferring LP location. In a second stage, we use the similarity of the events to calculate their relative positions. The analysis of the entire LP seismicity recorded between January 1997 and December 1999 suggests that a very large part of the LP event population, both deep and shallow, is generated by a small number of compact sources. Deep events are systematically composed of a weak high-frequency onset followed by a low-frequency wave train. Aligning the low-frequency wave trains does not lead to aligning the onsets indicating the two parts of the signal are dissociated. This observation favors an interpretation in terms of triggering and resonance of a magmatic conduit. Instead of defining fault planes, the precise relocation of similar LP events, based on the alignment of the high-energy low-frequency wave trains, defines limited size volumes. *INDEX TERMS:* 7294 Seismology: Instruments and techniques; 7280 Seismology: Volcano seismology (8419); 8419 Volcanology: Eruption monitoring (7280); *KEYWORDS:* LP events, multiplet, earthquake location, seismic amplitudes, Kilauea, Hawaii

Citation: Battaglia, J., J.-L. Got, and P. Okubo, Location of long-period events below Kilauea Volcano using seismic amplitudes and accurate relative relocation, *J. Geophys. Res.*, *108*(B12), 2553, doi:10.1029/2003JB002517, 2003.

1. Introduction

1.1. Background

[2] Kilauea Volcano is a basaltic volcano situated on the island of Hawaii. It is one of the most active and well known volcanoes in the world and its activity has been monitored by the Hawaii Volcano Observatory (HVO) since 1912. The monitoring network includes, at the time of our study, more than 60 seismic stations (Figure 1).

[3] The summit of Kilauea is characterized by the presence of a 5-km-wide caldera in which is located the Halemaumau pit crater. Two rift zones extend from the summit area to the southwest and to the east, forming narrow ridges that extend tens of kilometers offshore. Almost all known eruptions of Kilauea occurred either within its summit region or along its two rift zones [*Lockwood et al.*, 1999]. The last eruptions in the summit area occurred in 1972–1974 [*Lockwood et al.*, 1999] and 1981–1983 [*Klein et al.*, 1987]. However, since 1969, the activity of Kilauea has been dominated by eruptions in the East Rift Zone with two long duration eruptions: the 1969–1974 Mauna Ulu

[1]Also at U.S. Geological Survey, Hawaii Volcano Observatory, Hawaii National Park, Hawaii, USA.
[2]Now at Department of Geology and Geophysics, University of Wisconsin, Madison, USA.

0148-0227/03/2003JB002517$09.00

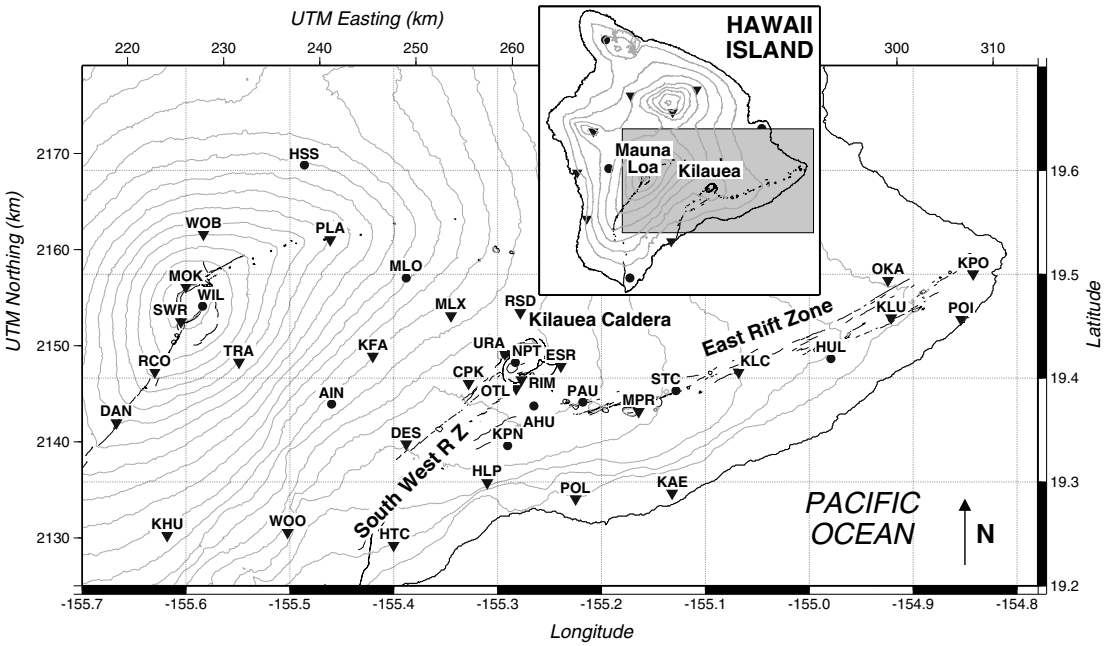

Figure 1. Map of the southeastern part of the island of Hawaii. Isolines are spaced every 200 m. Seismic stations of the monitoring network are represented as triangles in the case of single-component vertical sensors and solid circles for stations with horizontal sensors.

eruption [*Swanson et al.*, 1979; *Tilling*, 1987] and the Puu Oo eruption [*Wolfe*, 1988] which began at the end of 1983 and still continues at the time of writing.

[4] A model explaining how Kilauea works has been proposed by *Eaton and Murata* [1960] and the basic elements of that model still apply. More recently *Decker* [1987] and *Tilling and Dvorak* [1993] summarized new insights brought by advanced studies of several eruptions with modern techniques. The intraplate origin of Kilauea, as well as the origin of other Hawaiian volcanoes, is commonly attributed to the activity of a hot spot and to its interaction with the Pacific plate [*Wilson*, 1963; *Clague and Dalrymple*, 1987]. Magma rises by buoyancy from the mantle through a conduit located beneath the summit caldera until it reaches a magma reservoir situated between 7 and 2 km below the surface [*Delaney et al.*, 1990], mainly beneath the southern part of the summit region. The location of that reservoir is determined by the presence of an aseismic zone and inflation/deflation centers. From there, the transport of magma into the rift zones occurs through horizontal pathways at depth near 3 km [*Klein et al.*, 1987]. A model imaging Kilauea's underground plumbing system has been proposed by *Ryan at al.* [1981]. Such models largely rely on the use of seismic data and in particular catalog locations for tectonic events as well as for long-period events.

1.2. Long-Period Activity Below Kilauea

[5] In addition to sustained tectonic activity, the monitoring network of HVO commonly records long-period (LP) events related to the activity of Kilauea Volcano [*Koyanagi et al.*, 1987]. This type of event, commonly observed on active volcanoes, including basaltic and explosive systems, is particularly interesting for understanding their behavior as it is assumed that it actively involves fluids in its source mechanism [*Chouet*, 1996].

[6] Among the LP events related to Kilauea's activity, several categories are routinely distinguished at HVO according to their origin depth range (determined using arrival times) and spectral characteristics. The type of long-period event that has most commonly been recorded by the monitoring network during the past 10 years corresponds to events with an intermediate depth, in the range between 5 and 15 km below the surface. These events usually have a spectrum peaked between 1.0 and 2.0 Hz and most of the energy is found below 3.0 Hz (Figure 2a). We refer to these events as "deep" LPs in this paper. Shallower events, with an origin depth above 5 km, are subdivided in two categories depending on their spectral content: higher-frequency events with a spectrum peaked between 3 and 6 Hz and lower-frequency ones with a spectrum peaked below 3 Hz. We refer to these events as s1- and s2-type LPs, respectively. Examples of such events are shown in Figure 2. We note, however, that in the case of the s2-type event presented in Figures 2c and 2d, some high frequencies are also observed at stations close to the source, such as NPT, whereas more distant stations only display the low-frequency signature. Shallow events are less frequently recorded by the network as, due to their commonly very shallow depth (often above sea level), they only trigger a very small number of stations and are not recorded by the monitoring network. We do not use in the present paper the internal terminology of HVO where the s1-type, s2-type, and deep LPs are named A, B, and C type, respectively, since it leads to confusion with the classification defined by *Minakami* [1974].

[7] Despite the opportunity LPs present for studying the plumbing system of Kilauea, their location using traditional arrival time methods is usually inaccurate or impossible because of their emergent onsets. While techniques have been proposed using seismic arrays [*Almendros et al.*,

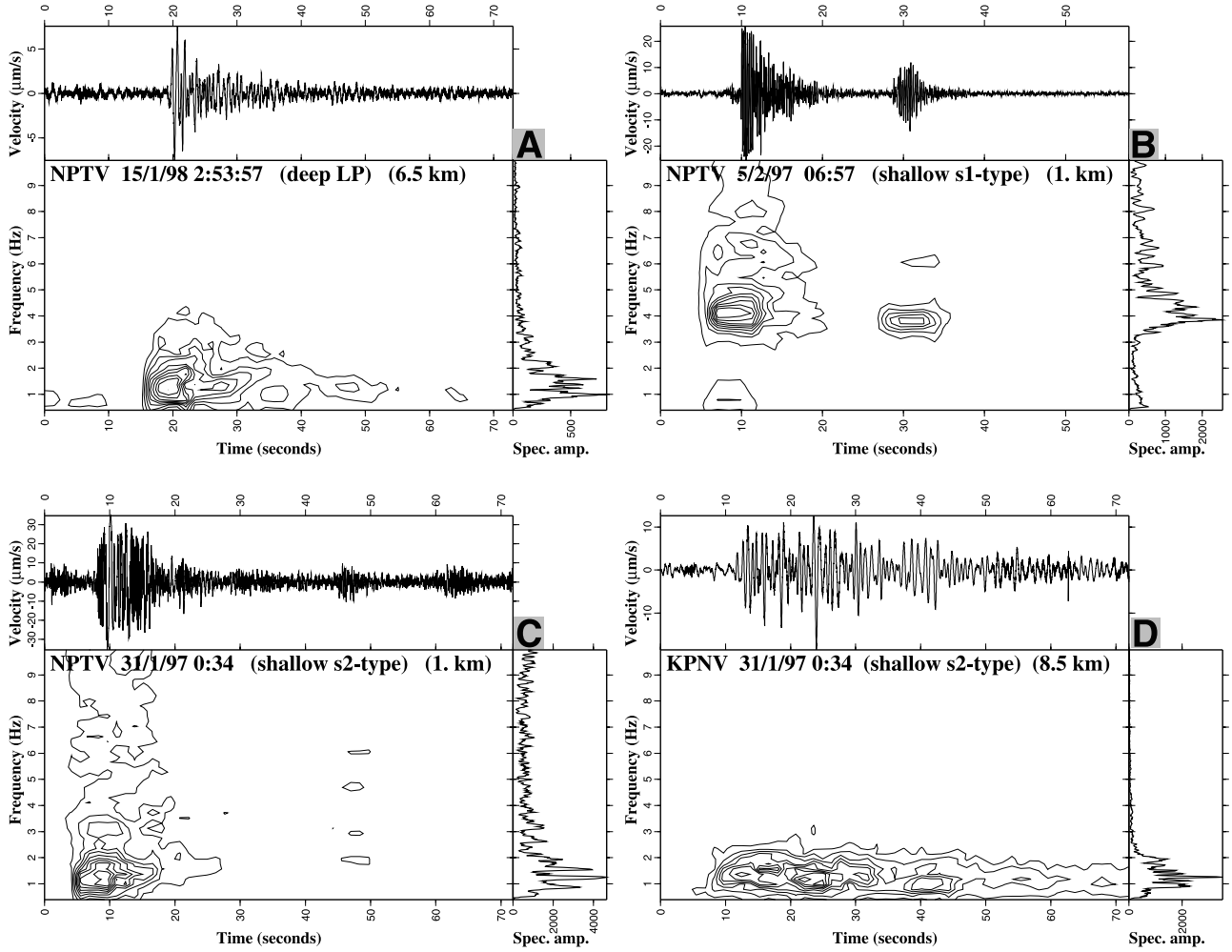

Figure 2. Examples of spectrograms and spectra for the different types of LP events observed below the summit of Kilauea. Spectrograms were obtained using a sliding window of 512 points (5.12 s), and spectra were calculated over the entire presented seismic traces.

2001a], this task is usually problematic using data from classical short-period volcano monitoring networks. Similarly to other volcanoes as Etna [*Falsaperla et al.*, 2002] or Pinatubo [*Ramos et al.*, 1999], we noticed in Hawaii the presence of similar LP events, deep (Figure 3) as well as shallow, suggesting the existence of multiplets. While this similarity of the waveforms suggests spatially close sources, those events are often given in the catalogs as widely scattered below the summit of Kilauea, over a volume with a diameter of about 5 km in the case of deep events and $0.7 \times 1 \times 2$ km ($x \times y \times z$) for the shallow ones. We attempt to improve upon these LP locations using seismic amplitude distributions and precise relative earthquake relocation techniques. We first present the two techniques we use and their characteristics when applied to LP events in Hawaii. In a second time, we present the results of their application to the entire LP activity which occurred from 1997 to 2001.

2. Data

[8] The HVO seismic monitoring network includes about 60 short-period stations installed across the island (Figure 1). Most of those stations are equipped with Mark Products L4 short-period seismometers with a natural frequency of 1 Hz. About 25% of the stations are equipped with a pair of orthogonal horizontal components. In addition to those stations, three three-component Guralp broadband stations and three three-component strong motion accelerometers are also included with the incoming data stream. Triggered data recorded digitally with a 100 Hz sampling rate are available on magneto-optical disks under the CUSP format since 1986. In the present work, we only use vertical components from short-period seismometers. Data presented in this paper were collected during the period from January 1997 to December 1999.

3. Location Using Seismic Amplitudes

[9] Because in most cases the onset of LP events is emergent and their arrival time estimates inaccurate, we propose to use seismic amplitudes to locate these events. It is, however, necessary to first correct for the possible presence of recording site effects. For that purpose, we use the coda amplification factors. The calculation of those

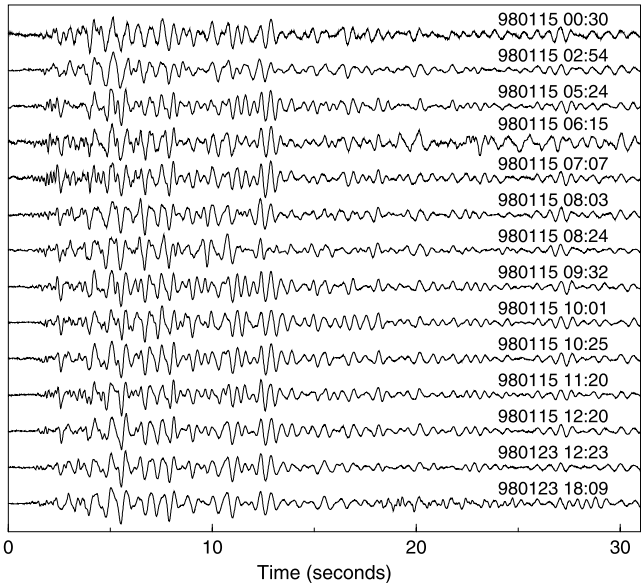

Figure 3. Example of similar deep long-period events recorded at station AHU, close to Kilauea's summit caldera (about 7 km from source) during January 1998. Similarity of the events is higher in later parts of the seismograms, in opposition with what is commonly observed for tectonic events.

factors is explained in detail in Appendix A. For each event, we plot the spatial distribution of the corrected amplitudes and look for the source at its origin assuming a given decay of the amplitude as a function of the hypocentral distance.

3.1. Spatial Amplitude Distributions

[10] The first step for drawing the spatial amplitude distribution for a given seismic event is to calculate its amplitude at each station of the network. For this purpose we use the RMS formula. It is actually much more stable than the peak to peak amplitude which may be strongly influenced by a single peak in the signal. RMS amplitude is also more stable than using the peak amplitude of the smoothed envelope of the signal. In the case of LP events, amplitudes are calculated in limited frequency bands over 20.48 s signal windows beginning with the approximate onset of the event as determined by catalog *P* wave arrival times. The choice of the frequency band depends on the spectral content of the event (Figure 2). We usually use the 1.0–3.0 or 1.0–4.0 Hz frequency band for deep LPs and the 1.0–6.0 frequency band for shallow LPs (s1 and s2 type). In the present work we use the coda factors calculated for the 1–3 Hz frequency band for correcting for recording site effects (Appendix A).

[11] Once corrected using coda amplification factors, the resulting amplitude distributions are usually smooth and simple. By simple we mean the distributions have a single maximum and decrease evenly in all directions. Figure 4 shows an example of normalized amplitude distributions obtained for two long-period events with different source depths. The distributions indicate the epicenter of the event and the density of the contours is representative of the depth of the source: dense contours for a shallow LP and sparse for a deep one.

3.2. Location Method

[12] On the basis of the simplicity of the obtained amplitude distributions, we apply a location program for inferring their source origin by approximating the decay of the amplitude as a function of the hypocentral distance. This method was originally developed on the Piton de la Fournaise volcano [*Battaglia and Aki*, 2003] and was used successfully for locating eruption tremor sources. The decay of the amplitude is approximated using the body wave amplitude decay which assumes that the amplitude

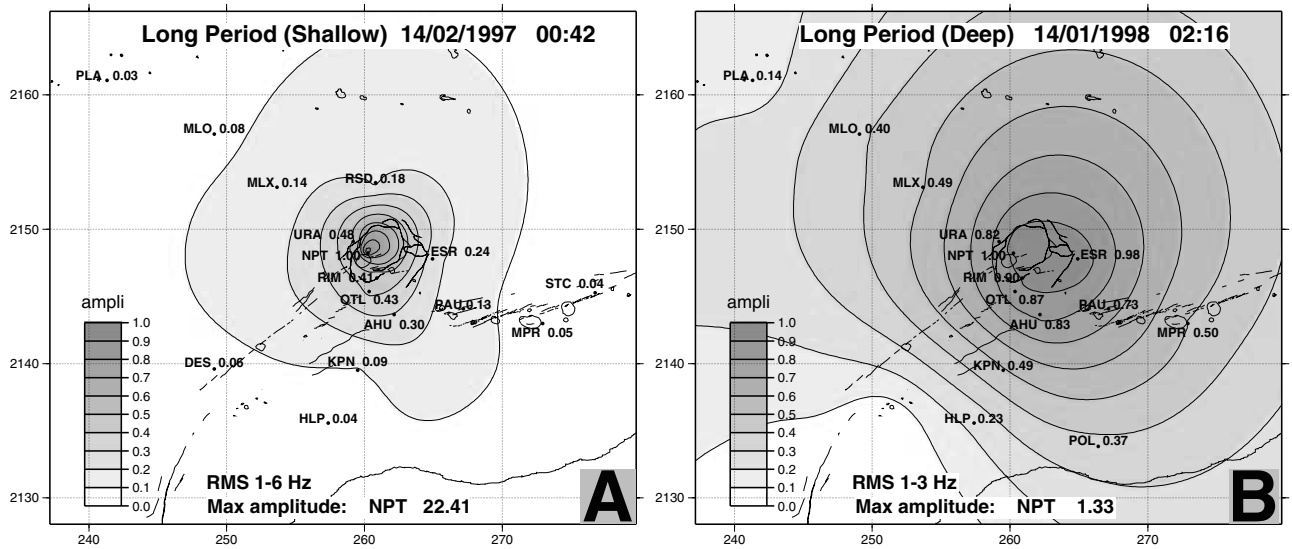

Figure 4. Normalized amplitude distributions for two long-period events observed under the summit of Kilauea. Contours give an estimation of the epicentral source location and the density of those contours suggests different focal depths: (a) dense contours for a shallow LP event and (b) sparse for a deep event.

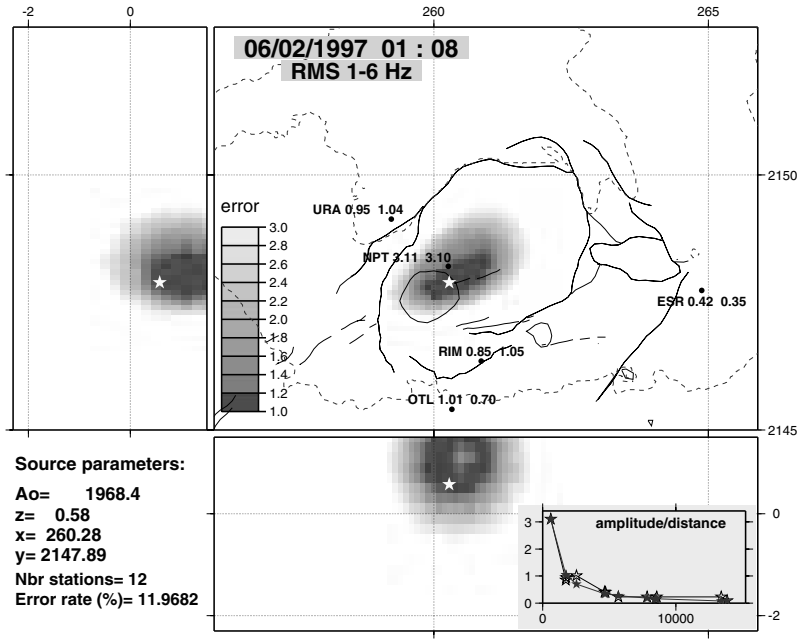

Figure 5. Location in the 1–6 Hz frequency band of a shallow s1-type LP event. The best source is plotted as a white star on the plane projection showing the summit of Kilauea. E-W and N-S cross sections are also shown. Coordinates are UTM kilometric coordinates, altitude is in kilometers and 0 is sea level. Contours of normalized error rate are plotted and observed and modeled amplitudes are indicated beside the name of each station. The decays (observed and modeled) of the amplitude as a function of the hypocentral distance are also shown.

decreases proportionally to the inverse of the hypocentral distance:

$$A(r) = A_0 \frac{e^{-Br}}{r} \tag{1}$$

with

$$B = \frac{\pi f}{Q\beta} \tag{2}$$

where r is the hypocentral distance from the seismic source, A_0 is the source amplitude, f is frequency, β is wave velocity and Q is the quality factor for attenuation. For LP events, as we usually consider frequencies between 1 and 6 Hz, we use $f = 3$ Hz, $Q = 66$ [*Koyanagi et al.*, 1992] and $\beta = 2300$ m/s. We, however, note that these values do not have a great influence on the result of the locations as the geometrical expansion of the wave front predominates over the anelastic attenuation. For each seismic event the search for the best source is done in two parts [*Battaglia and Aki*, 2003]. First, we try various trial source amplitudes at each point of a three-dimensional (3-D) grid and use equation (1) to calculate the amplitude at each station of the network. The discrepancy between the calculated and observed amplitudes is evaluated using a squared differences criterion and a temporary best source is obtained for the quadruplet which minimizes the error function. Next, the parameters of that solution are improved using a gradient method. For the best source we define an error percentage and thanks to the grid calculation, we can define at each point of the 3-D grid the minimum error among all trial values of the source amplitude. For each individual location we plot the projections of the normalized minimum error on the north-south and east-west cross sections and on the plane view as shown in Figure 5.

3.3. Validation for the Location of LPs in Hawaii

[13] Since the amplitude location method presented above is relatively new and has until now only been used at the Piton de la Fournaise volcano, in order to validate its use in the case of Hawaii we applied it to events that occurred below the summit of Kilauea and for which locations are available using independent techniques. We applied it to shallow LP events recorded in February 1997. From 30 January to about 15 February, a period of enhanced LP activity, with thousands of events per day, was observed below the Kilauea summit caldera. From 8 to 12 February, three dense seismic arrays, including 41 three-component stations and 22 and 12 vertical component seismometers, respectively, were installed in the Kilauea Caldera as part of a joint Japan-U.S. experiment. Data from those antennas were used by *Almendros et al.* [2001b] for locating LP sources. These authors showed that all the LP seismicity was generated in a source region, with dimension about $0.6 \times 1.0 \times 0.5$ km, located along the eastern and northeastern flank of Halemaumau pit crater at a depth of about 200–400 m.

[14] Among the 2155 LP events that triggered the monitoring network between 1 and 15 February 1997, we processed about 1553 events. Because of the very shallow depth of the events, traces were saturated at stations close to the source for 752 events. RMS amplitudes were calculated between 1 and 6 Hz for the 801 remaining events and our location method was applied to the obtained amplitude sets.

Figure 5 shows the result obtained when applying our program to one of those LP events. The source is approximately found in the area of activity defined by *Almendros et al.* [2001b]. The darker area on the plot corresponds to the volume were the normalized error is between 1.0 and 1.2 time the minimum error obtained for the best source. This area is elongated in the SW-NE direction mainly due to the absence of any seismic station northeast of the caldera but the result clearly points out the activation of a shallow source situated northeast of Halemaumau pit crater, a few hundred meters below the surface. Among the 801 located events, 47 were deep LPs with sources about 4 km below sea level and the remaining 754 shallow LPs had sources above sea level. The locations for the 754 events form a cloud above sea level with shape similar to the darkest area in Figure 5 (these locations are shown in Figure 8 with other LP locations). The centroid of that cloud is found at coordinates $X = 260.59 \pm 0.46$, $Y = 2147.95 \pm 0.33$ and $Z = 0.75 \pm 0.35$ (UTM coordinates), close to the location presented in Figure 5. Despite a reduced precision because of the sparse station coverage, our method gives results in good agreement with the results obtained using seismic antennas. Also, we note that the application of our method to other events with signals saturated at stations close to the source gives very similar locations. These results emphasize the possibility of using seismic amplitudes for locating LP events under the summit of Kilauea.

4. Precise Relative Relocation of the Events

[15] The next step for improving the location of similar LP events is to use the similarity of the waveforms in order to apply relative location methods. This type of method has commonly been applied to the precise relative relocation of tectonic events on volcanoes [*Frémont and Malone*, 1987; *Got et al.*, 1994; *Gillard et al.*, 1996; *Got and Okubo*, 2003] but rarely to LP events [*Wolfe et al.*, 2003]. Similar earthquakes occur when both source processes and hypocentral locations are similar. The similarity of waveforms allows the accurate calculation of time delays between traces recorded at the same receiver. The spatial proximity of the hypocenters allows one to linearize the relative location problem. We follow the linear approach described by *Got et al.* [1994] to compute the relative positions of the similar earthquakes studied in this paper.

[16] The processing follows three steps: identification of groups of similar events, computation of time delays between similar pairs, and calculation of the relative positions. The first two steps require defining the degree of similarity between pairs of events. For the identification of multiplets, we use the linear cross correlation and for delay computation we test both linear cross-correlation and cross-spectral analysis [*Got et al.*, 1994]. In the case of tectonic events, the processing is usually done using very short signal windows of 1.28 or 2.56 s starting with the *P* arrivals. However, in the case of LPs, it is often difficult to define precisely the *P* arrival and the similarity is not as high at the beginning of the events as in its entire waveform (Figure 3). For those reasons we use 20.48-s-long windows for the processing. Also, in the case of tectonic events, the extraction of signal windows for delay computation is done using the picked arrival times. For LPs, as the uncertainty on the arrival times is large, we only use data extracted in such a way for the classification. Once families of similar events have been defined, the extraction of signal windows inside each family is done assuming the hypocenter of each event is at the centroid of the locations given by the amplitude method. Approximate onsets are obtained by computing travel times between the centroid and each station, the origin time of each event is chosen so that the calculated onset at AHU station matches the catalog pick.

4.1. Multiplet Selection

[17] In order to build families of similar LP events, we compute the generalized cross-correlation matrix for the available LP events. The computation is done separately for deep and shallow events according to their amplitude locations. To limit the influence of noise, cross correlation is performed after band pass filtering the signals between 0.5 and 5 Hz in the case of deep LPs and between 1.0 and 8.0 Hz for shallow ones. The number of events assigned to a family depends on the criterion used for defining the similarity. In the present work, we use two criteria.

[18] 1. We assume that two events are very similar if they have a correlation higher than 0.8 at least at three stations of the network (criterion C1). Families defined this way give precise relative relocations because of the high number of delays between the events and are used to define precisely the shape of the active structures.

[19] 2. This criterion is, however, very restrictive as we consider large signal windows which tend to reduce the similarity and also because the similarity between LP events is generally lower than between tectonic events. In order to group a maximum number of events we relax the correlation threshold and assume that two events belong to the same multiplet if they have a correlation higher than 0.6 at least at three stations (criterion C2).

4.2. Calculation of the Delays

[20] The calculation of delays between pairs of similar events is based on aligning traces at the different stations of the network. This computation is done for each pair of events (doublet) within a multiplet. A first solution for calculating delays is to use the linear cross correlation. Signals are first band-pass filtered in the same way as for the classification and the best alignment is obtained for the maximum of the cross-correlation function calculated on 20.48 s windows. An alternate solution is to use the cross-spectral analysis which leads to a subsample precision in the delay calculation [*Jenkins and Watts*, 1968]. In that case, delays are proportional to the slope of the cross-spectrum phase and the computation is carried out from the weighted linear adjustment of the phase of the cross spectrum [*Poupinet et al.*, 1984]. However, instead of the tectonic events which have a wide spectrum, the one for LP events is much narrower and the slope of the cross-spectrum phase is actually estimated from a very narrow spectral window (between 1.0 and 3.0 Hz for deep LPs), which tends to increase the uncertainty of the delay estimation. To limit this effect, hypothesizing that the cross spectrum phase is stationary with time elapsed along the seismogram, we use long signal windows (20.48 s, i.e., 2048 samples) to compute the cross-spectrum phase. This allows the cross-spectrum phase to be computed with a significant number

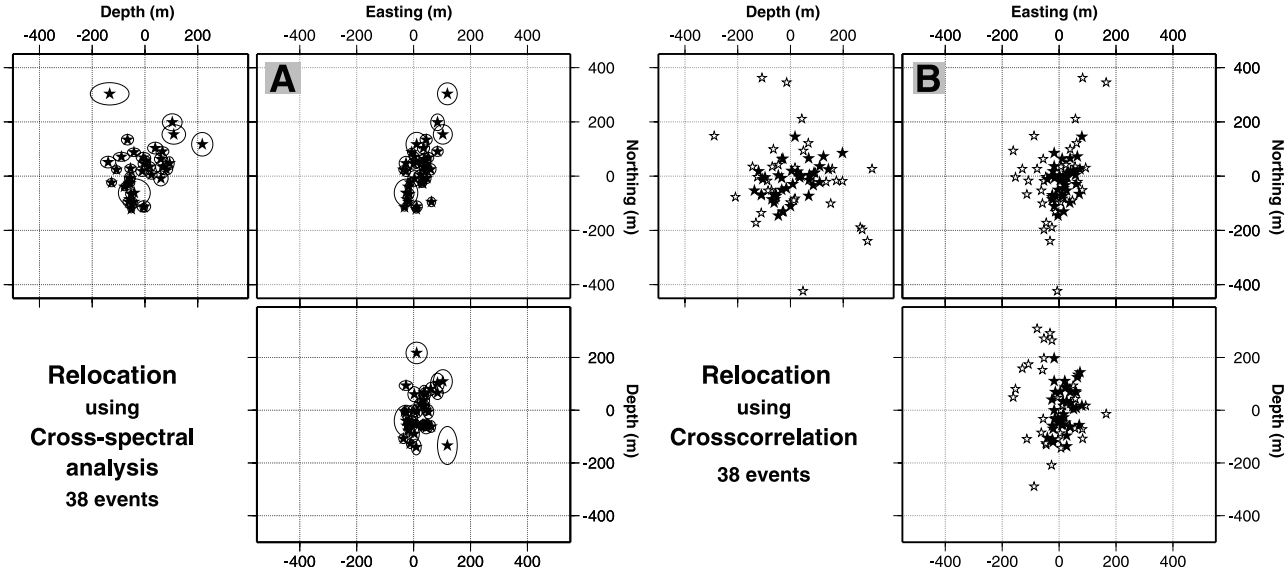

Figure 6. Relocations for 37 very similar deep LP events recorded in January 1998, when calculating delays (a) with the cross-spectral analysis and (b) with linear cross correlation. Ellipse errors deduced from Monte Carlo simulations are plotted for relocations obtained using cross-spectral analysis. The average horizontal precision for these relocations is about 20 m and vertical is about 30 m. On Figure 6b, relocations for 54 less similar events are also plotted as open stars.

of samples in the frequency band of interest and therefore to obtain an accuracy of time delay measurements better than 5 ms.

[21] Because of the almost monochromatic aspect of the traces, misalignments of one or several periods (“cycle jumps”) are sometimes encountered leading to aberrant delays. Since we use traces extracted assuming all the events in a multiplet have a common hypocenter, delays at the different stations for a given doublet are similar to each other except if traces are improperly aligned. Because in the extraction process an uncertainty remains concerning the origin time of the events, those delays are usually not centered around zero making difficult the detection of cycle jumps. For this reason, data are extracted a second time after adjusting the origin time of each event so that all delays corresponding to correct alignments are found close to zero. Then, in the delay calculation, a limitation is introduced in order to avoid large values, and so to eliminate cycle jumps.

[22] We found that for very similar events (criterion C1), both the cross-correlation and the cross-spectral analysis give comparable good quality relocations (Figure 6). However, for less similar events (criterion C2), the calculation of delays using cross-spectral analysis lead to poorly constrained relocations because of misalignments between less similar traces. The cross-correlation analysis appears to be more robust for calculating delays in the case of less similar pairs.

4.3. Relocation

[23] The last step in the relative relocation process is to use the delays for calculating the relative position of the events. Because of the spatial proximity of the hypocenters, we may assume that the rays from all similar events to a given station are parallel and that the velocity in the source region is constant. We assume that the time delay Δt_{ij}^k between traces recorded for two neighboring events i and j at the same station k is not perturbed by velocity anomalies along the ray path and contains only information related to the difference in the location of the events i and j. It is therefore linearly related to the relative source position vector $\mathbf{r}_{ij} = (x_{ij}, y_{ij}, z_{ij})^T$:

$$\Delta t_{ij}^k = \Delta t_{orij} + \mathbf{r}_{ij}.\mathbf{s}^k = \Delta t_{\mathrm{orij}} + x_{ij}s_x^k + y_{ij}s_y^k + s_{ij}s_z^k \qquad (3)$$

where $\mathbf{s}^k = (s_x^k, s_y^k, s_z^k)^T$ is the slowness vector for the station k, and Δt_{orij} is the origin time difference for the event pair (i, j). Equation (3) can be formulated as a linear inverse problem in which the parameters of the model are $\mathbf{m} = (x_{ij}, y_{ij}, z_{ij}, \Delta t_{\mathrm{orij}})^T$:

$$\mathbf{Gm} = \mathbf{d} \qquad (4)$$

where $\mathbf{G}$ is the matrix containing the s^k partial derivatives of Δt_{ij}^k relative to the unknown vector $\mathbf{m}$, and $\mathbf{d}$ is the data vector containing the time delays. It is solved in a least squares sense by using the normal equation inversion scheme:

$$\mathbf{m} = \left(\mathbf{G}^T\mathbf{C}_d^{-1}\mathbf{G}\right)^{-1}\mathbf{G}^T\mathbf{C}_d^{-1}\mathbf{d} \qquad (5)$$

where C_d is the data covariance matrix built from the time delay uncertainty, using the Cholesky decomposition of $\mathbf{G}^T\mathbf{C}_d{}^{-1}\mathbf{G}$ (see *Got et al.* [1994] for details). The use of delays calculated for all possible and different event pairs leads such a system to be strongly overdetermined and improves the accuracy of its least squares solution. Aberrant delays are rejected by an appropriate statistical analysis of the residuals during the relocation steps.

[24] In order to estimate the uncertainty in the relocation, we use a Monte Carlo simulation assuming a Gaussian error of about 10 degrees on both takeoff and azimuth angles and

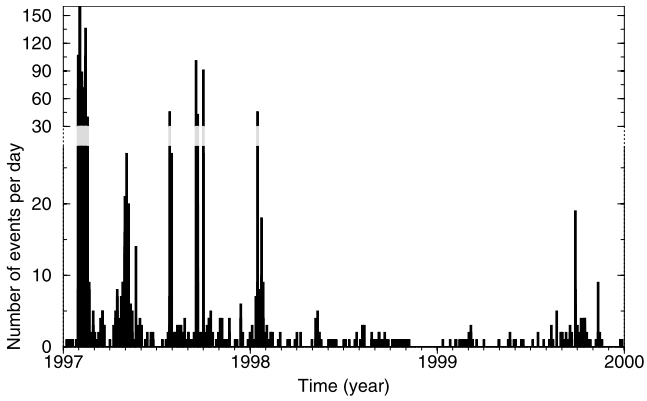

Figure 7. Number of LP events per day between January 1997 and December 1999 (from catalog). Vertical scale is different for the upper and lower part of the plot. Two values are out of range in February 1997 with 372 events on 1 February and 288 on 2 February. Most of the events are deep LPs, except during February 1997 when mainly shallow LP events were observed.

10 ms on the delays. Uncertainties in x, y and z are computed by running up to 200 relocation processes after adding the Gaussian errors and by calculating the standard deviation over the obtained relocations. This approach is preferred to the use of the root square of the diagonal elements of the variance-covariance matrix of the model estimates $\mathbf{C}_m = \mathbf{G}^T\mathbf{C}_d^{-1}\mathbf{G}$ (least squares uncertainties) as this last solution tends to underestimate errors by not taking into account uncertainties in $\mathbf{G}$ [*Got et al.*, 1994]. Examples of 67% confidence error ellipses calculated using the Monte Carlo method are given in Figure 6a and are representative of the uncertainties commonly obtained for the relocation of deep and shallow LPs, average uncertainties are about ±30 m in horizontal and ±35 m in vertical.

5. LP Activity Between January 1997 and December 1999

5.1. Time Distribution of the Events

[25] We applied our location and relocation methods to LP events recorded between January 1997 and December 1999. During that period the network recorded 3767 LP events according to seismic catalogs, about 2437 shallow and 1330 deep events. The time distribution of those events is plotted in Figure 7. Almost all the shallow events occurred between 30 January and 15 February 1997 during a phase of very high LP activity that followed a large deflation of Kilauea's summit caldera (30 μrad) and a short-lived fissure eruption in Napau crater on 30–31 January. In contrast, the deeper LP seismicity is more scattered over the period of study, although with most of the events occurring between February 1997 and January 1998. Also, most of the deeper LPs occurred during a small number of periods of enhanced LP activity lasting for only several days. LP activity was generally very low from the end of January 1998 until August 1999, with a small increase in the number of events in October and November 1999.

[26] Among the recorded events we extracted all of the 1330 available deep events and 1750 shallow LPs. We only selected part of the shallow LPs because a very large number of the triggered events were multiple events separated by very short delays or overlapping each others. Figure 8a shows the catalog locations for all the LP events. Shallow events (both s1 and s2 type) are clustered in a volume above 1 km below sea level and below the northeastern part of Halemaumau pit crater. The deep LPs are

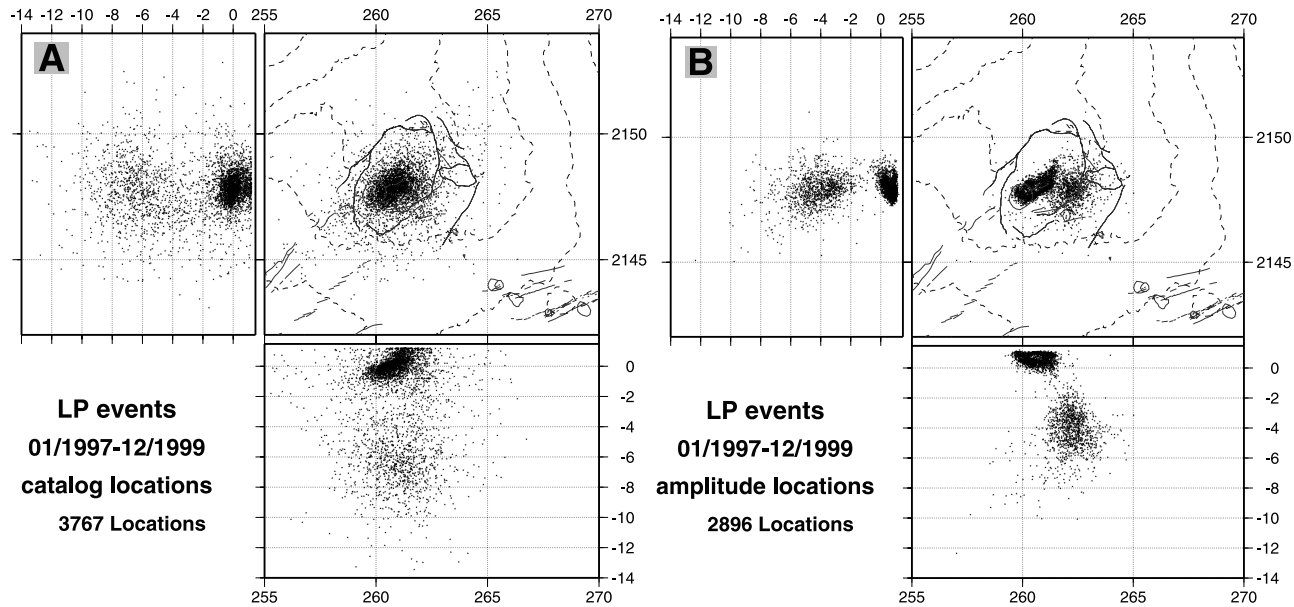

Figure 8. Comparison between (a) catalog locations and (b) locations obtained using seismic amplitudes for all events recorded between January 1997 and December 1999. Geographic coordinates are UTM coordinates and altitude is in kilometers.

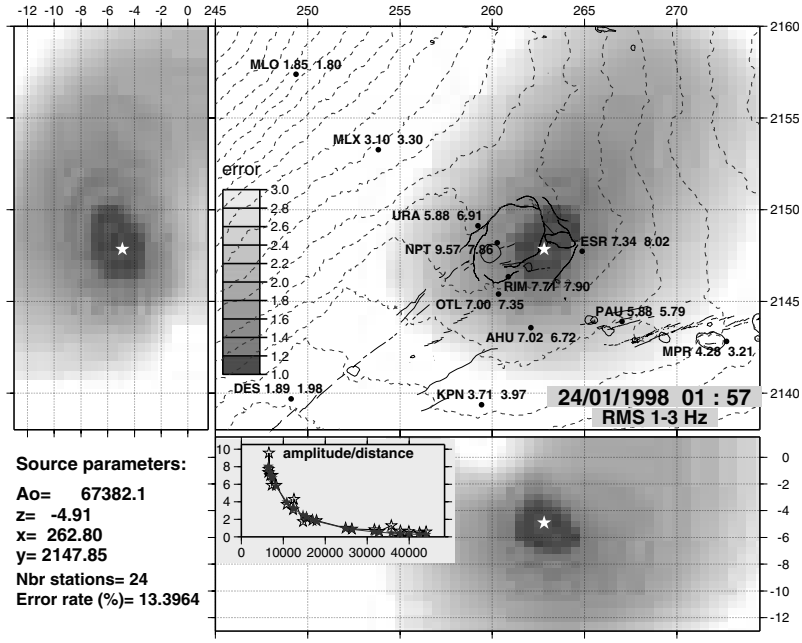

Figure 9. Location of a deep LP event using seismic amplitudes calculated in the 1–3 Hz frequency band. Normalized error contours are elongated to the northeast due to the station coverage.

scattered over a wide area below the summit of Kilauea, roughly between 3 and 10 km below sea level.

5.2. Amplitude Location

[27] We applied our amplitude location method to the 3080 selected events. Figure 8b shows the locations obtained for 2896 events, including 1746 shallow sources and 1150 deep ones. Figure 9 presents an example of the location of a single deep LP event. The amplitude location method allowed the location of almost all shallow events, including those saturated at some stations. However, for deep events, we could not locate properly 160 events, mainly because the available data did not allow a sufficient station coverage, leading to large uncertainties in the locations. Most of the events (139 of the 160) for which no satisfactory locations could be obtained were recorded between mid-1998 and the end of 1999. Indeed, no constraints on the source locations could be obtained in a 120° quadrant northeast of the summit because stations ESR and PAU (see Figure 1 for location) were not working

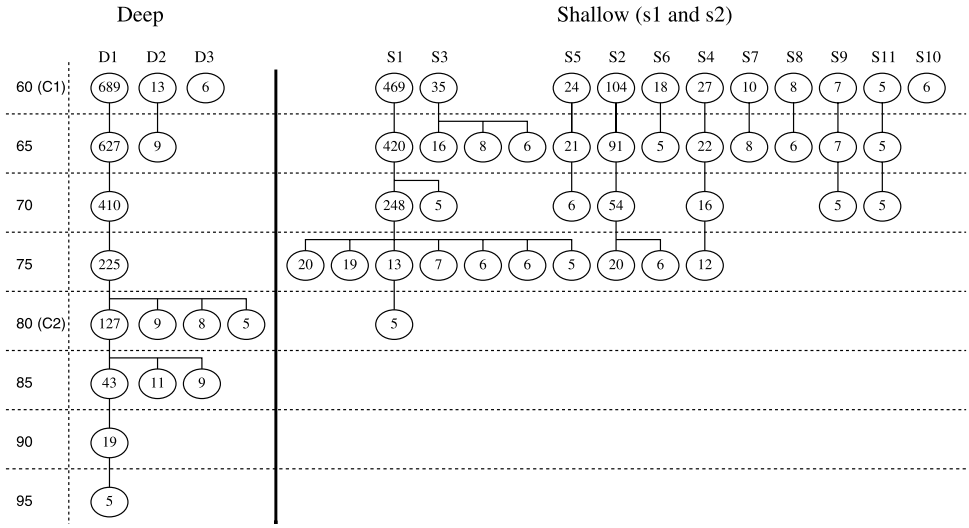

Figure 10. Number of events in each multiplet as a function of the threshold used for defining the similarity between the events. For example, the 60 (C1) corresponds to criterion C1 and means that events are assumed to be similar if the cross correlation has a value higher than 0.60 at least at three stations of the network; 65 if the cross correlation has a value higher than 0.65 at least at three stations. Classification for deep LPs is on the left part of the plot and on the right for the shallow ones.

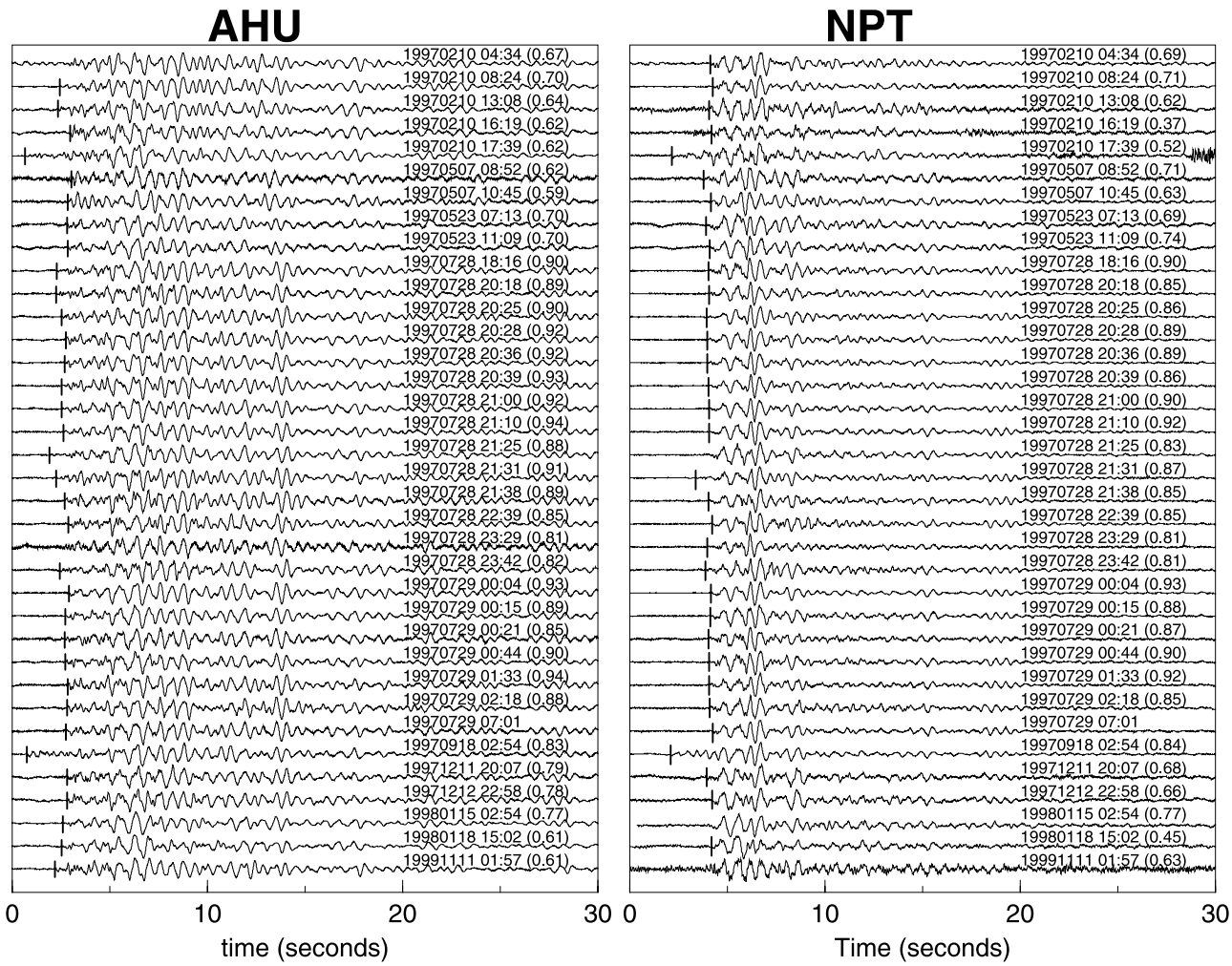

Figure 11. Similar deep LP events recorded between January 1997 and December 1999 and belonging to multiplet D1. (left) Traces recorded at station AHU about 8 km from source (hypocentral distance). (right) Traces at station NPT about 6 km from source. Same events, in the same order, are plotted on both parts. Traces are aligned and not filtered, the value in parentheses close to each date corresponds to the normalized cross correlation calculated over 40 s time windows between each trace and the trace recorded at 0701 LT, 29 July 1997. Vertical bars at the beginning of each event correspond to the approximate first arrival. Note that the bodies of the seismograms are aligned but not the first arrivals.

at that time. This absence of constraints causes a wide scattering of the sources around a mid position corresponding to the deep cluster of events observed in Figure 8b. Locations for those poorly constrained locations are not shown.

[28] Figure 8b indicates the presence of two main clusters of sources, a shallow and a deep one, grouping almost all the shallow (s1 and s2 type) and deep LPs as defined by the HVO classification. In the case of deep LPs, in contrast to the catalog locations which are widely scattered, almost all sources cluster in a single cloud situated below the eastern part of Kilauea's caldera at about 4 km below sea level. Despite the remaining scatter, amplitude locations suggest the activation of a specific source volume under the eastern part of the caldera during all the period of our study. For shallow LPs the clustering is also improved compared to catalog locations and the method also suggests the activation of a specific source volume extending northeast of Halemaumau.

5.3. Classification

[29] In order to identify groups of similar events we compared traces using linear cross correlation as mentioned earlier. Comparisons were done separately for the 1330 deep events and for the 1750 shallow ones. Figure 10 shows the number of events associated to each multiplet as a function of the threshold used for defining the similarity between the events.

[30] In the case of deep events, three different multiplets can be defined. Multiplets D2 and D3 include few events and the similarity between the events is rather poor. The main multiplet D1 includes up to 689 events according to criterion C1 and represents about 52% of all deep events. According to criterion C2, multiplet D1 is divided into

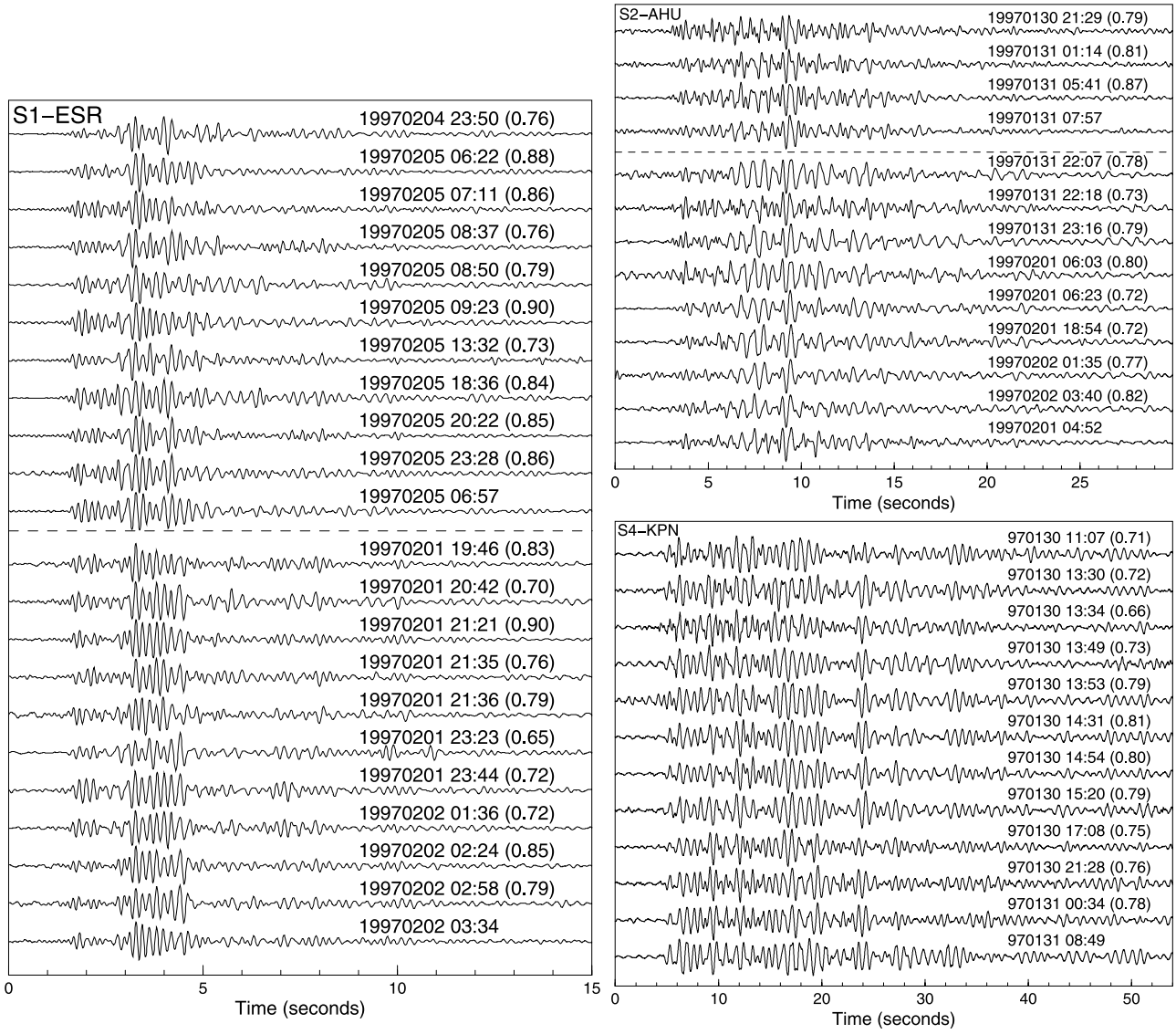

Figure 12. Example of similar shallow LP events belonging to multiplets (left) S1, (top right) S2, and (bottom right) S4. Timescales are different for each plot. Traces were recorded at station ESR, about 5 km from source for multiplets S1; at station AHU, about 5 km from source for S2; and at station KPN, about 8 km from source for S4. All traces were band-pass-filtered between 1.0 and 8.0 Hz. The value in parentheses close-by each origin time corresponds to the value of the normalized linear cross correlation between each trace and a reference trace chosen for its good similarity with most of the events. For multiplet S1, the 11 upper traces belong to the 13-member subfamily at threshold 75 in Figure 10, and the reference trace is the event above the dashed line; the 11 lower traces belong to the 20-member subfamily at the same level of similarity, and the reference trace is the lowermost one. Similarly, traces for multiplet S2 are affiliated to two different subfamilies. For S4, cross-correlation values were calculated with the lowermost trace.

four subfamilies. The similarity between events belonging to the different subfamilies is, however, sufficient for calculating accurate delays between the traces. Figure 11 displays traces for same events belonging to multiplet D1 recorded over all the period of our study at stations AHU and NPT, first arrivals are indicated by vertical lines. Traces were aligned using 20.48 s low-pass-filtered signal windows and the similarity is usually high according to cross-correlation values. Most of the time, we note the presence of a higher-frequency phase preceding the low-frequency wave train. The presence of such a higher frequency onset is a characteristic commonly observed for LPs [*Chouet et al.*, 1994]. In our case, however, aligning traces using large windows leads to aligning the most energetic and low-frequency part of the signal while the weaker part corresponding to the onset is not aligned. Similar variability in the timing between the high- and low-frequency phases was observed for hybrid earthquakes at Shishaldin volcano [*Caplan-Auerbach et al.*, 2002].

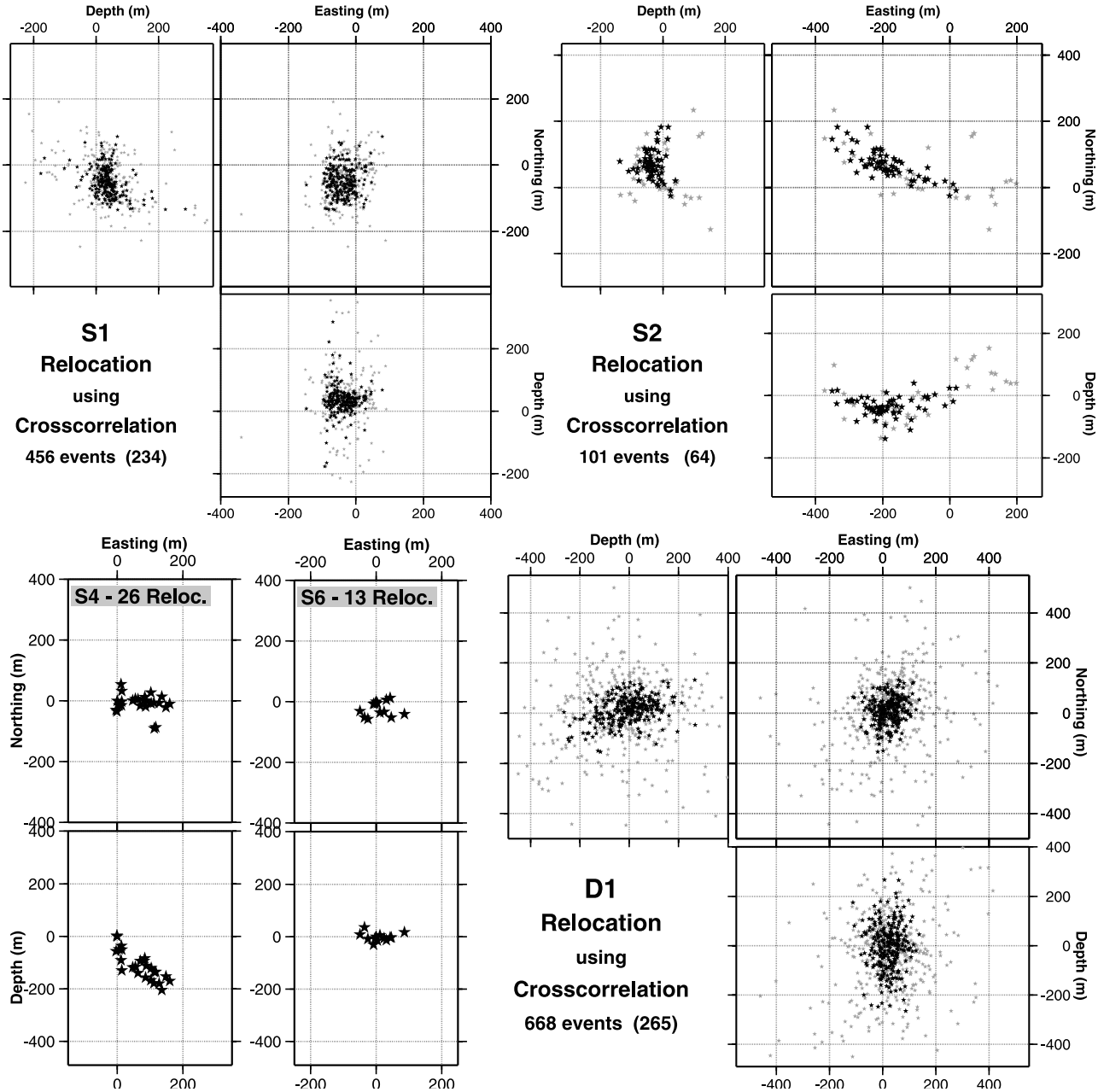

Figure 13. Relocations for multiplets D1, S1, S2, S4, and S6 using cross correlation for the calculation of delays. For multiplets D1, S1, and S2, map view and north-south and east-west cross sections are shown, the events relocated using a high number of delays are plotted as solid (the number of such events is indicated in parentheses), and the other relocated events are plotted as grey stars. For multiplets S4 and S6, all relocations are shown only on map view and east-west cross section.

[31] In the case of shallow LPs, families of similar events can also be defined despite a similarity between the events lower than for deep ones (Figure 10). Eleven multiplets including at least five events can be defined grouping a total of 713 events (41% of the selected shallow events), with five multiplets including more than 20 events according to criterion C1. The largest multiplet S1 groups 469 LPs and S2 groups 104 LPs. Example of events belonging to multiplets S1, S2 and S4 are shown in Figure 12. All shallow multiplets except S8 include only events that occurred during the period of enhanced LP activity between 30 January and the end of February 1997.

5.4. Relative Relocation

[32] We applied the relocation method to the different multiplets defined above. In each case, traces were extracted supposing all events in a family originate at the centroid of the locations obtained using amplitudes. For deep events, the UTM coordinates (expressed in kilometers) of the centroid are $X = 262.29$, $Y = 2147.70$, and $Z = -4.38$. For shallow events, amplitude locations suggest different

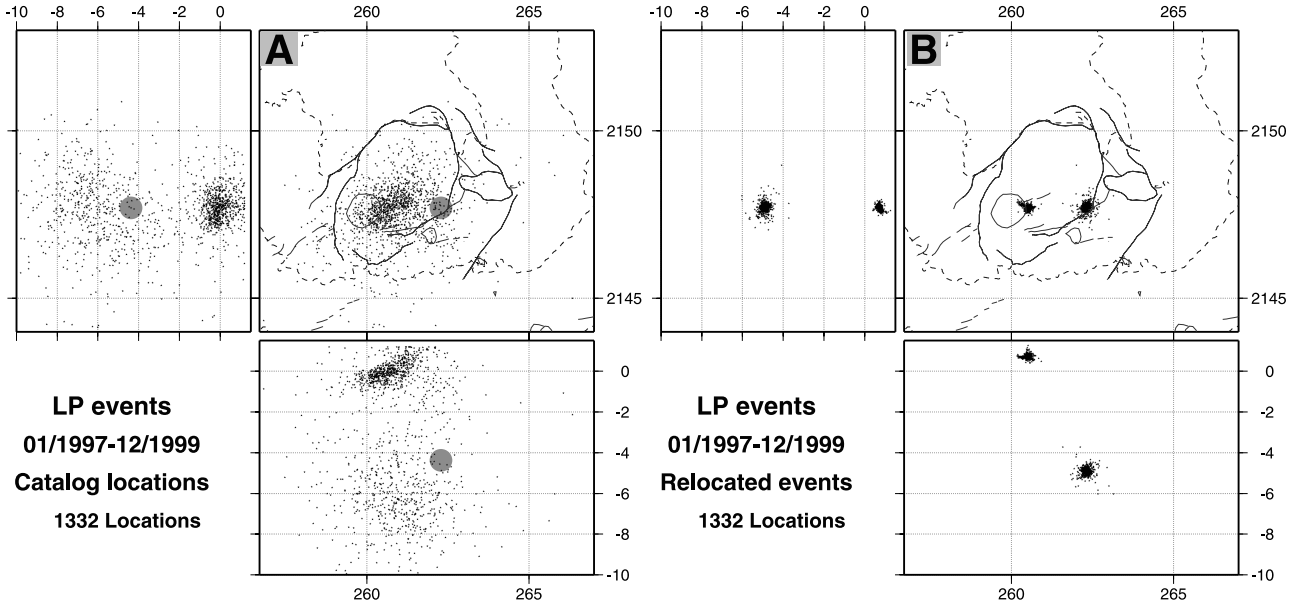

Figure 14. Comparison between locations obtained for (b) the relocated events and (a) the original catalog locations for the same events. Map view and north-south and east-west cross sections (depth in km). The position of the cluster of deep events is added on the right plot for comparison, its absolute location was determined from amplitude locations.

centroids depending on the multiplet. This variability may, however, be related to the uncertainty in the locations and for the extraction of data we assume all shallow multiplets have a common centroid chosen at the mean position of all shallow amplitude locations: $X = 260.55$, $Y = 2147.72$, and $Z = 0.73$. We, however, noticed that the absolute location of each multiplet does not have in this case a great influence on the shape defined by the relocated events. Figure 13 shows the relocated events for multiplets D1, S1, S2, S4, and S6. The relocations for the other families, both deep and shallow do not show any particular shape as events are grouped into small clouds.

[33] In the case of multiplet D1 (Figure 13), the best relocations, obtained using a high number of delays, define a slightly vertically elongated shape corresponding rather to a volume rather than to a fault plane. The dimensions of that volume are about 400 m high and about 200 m wide and exceed by far the uncertainties on the relocations that are about 30 m horizontally and 35 m vertically. The poorer quality relocations increase the scattering but do not change much the pattern defined by the relocations. According to the large number of relocated events (667), the spatial extent of the relocations is small as compared to structures defined by the relocation of tectonic events. For shallow LPs, the relocated events for multiplet S1 define a horizontally elongated volume about 160 m long, 160 m wide and 80 m high. For S2, the relocations also define a horizontally elongated structure, about 400 m long, 80 m wide and 100 m high. For S4 and S6, the defined structures are also slightly horizontally elongated with a small spatial extent.

[34] Figure 14 shows all the relocated events and emphasizes the presence of a limited number of LP sources as already suggested by the amplitude locations in Figure 8. In the case of shallow LPs, the clustering was already suggested by catalog locations, however, in the case of the deep LPs, sources were widely scattered whereas our method indicates they are densely clustered.

6. Discussion and Conclusions

[35] We present two methods to improve the location of shallow and deep long-period events recorded below Kilauea Volcano. In order to improve the absolute location, instead of using arrival times which are often unclear, we use seismic amplitudes corrected for recording site effects. Locations are obtained by approximating the decay of the amplitude as a function of the hypocentral distance by the amplitude decay of body waves. The presence of large families of similar events allows to apply precise relocation techniques in order to improve the relative position of the events.

[36] The analysis of the LP seismicity that occurred from January 1997 to December 1999 shows that a large part of this type of seismicity, deep events as well as shallow, is generated by a small number of sources. About 52% of the deep LPs that occurred during the period of study can be considered as similar and belong to one multiplet. The use of seismic amplitudes greatly improves the clustering in the absolute location of these events and their precise relative relocation defines a vertically elongated volume with most of the events found in a volume about 400 m high and 200 m wide. The typical uncertainty on the individual relocations is about 30 m horizontally and 35 m vertically. Also, most of the remaining events, despite having nonsimilar waveforms, appear to originate from the same volume according to amplitude locations. Instead of a scattered deep LP activity, our analysis suggests the repetitive activation of a unique source during a period of at least three years. Assuming that LP activity is reflecting fluid transfers at depth, our results suggest

that transfers capable of generating long-period seismicity are very localized and that probably most of fluid transfers occur aseismically in the volcanic edifice. It is therefore impossible to map the magma path in its continuity by merely locating these LP events. However, there is probably a large number of magma-filled cracks in an active volcano like Kilauea. It seems therefore that only few locations meet the geometric, stress, thermal and pressure conditions required for generating enough LP seismic energy to be recorded at the surface.

[37] In the case of shallow LPs the similarity between the events is lower than for the deep ones. Multiplets can, however, still be defined and delays can be used for relocating the events. In this case also a large part of the seismicity appears to be originating from a small number of sources. The relative position of those sources cannot be precisely determined using only data from the short-period monitoring network but individually the spatial extent of those sources is only a few hundred meters.

[38] Instead of tectonic events, the relocation of LPs does not clearly define fault planes but rather volumes, vertically elongated in the case the deep LPs and rather horizontally elongated in the case of shallow ones. The occurrence of LPs is commonly attributed to the resonance of a fluid filled volume in response to a trigger. The nature and shape of the resonant structure vary among the different authors: rectangular cracks for *Aki et al.* [1977], *Chouet* [1981], spherical source for *Kubotera* [1974], *Crosson and Bame* [1985] or cylindrical source for *Chouet* [1985]. Various mechanisms have also been proposed for the origin of the oscillations such as transient disturbances in the flow produced by nearby earthquakes, fluid heterogeneities or changes in channel geometry [*Julian*, 1994], disturbance in the volcanic conduit similar to a water hammer effect [*St. Lawrence and Qamar*, 1979] or unsteady flow [*Ferrick at al.*, 1982] for example. Independently of the details of the model, we may assume that the main part of the LP waveform corresponds to the resonance of a fluid filled volume and then relocating LPs using delays calculated almost with the entire waveforms implies that we do not relocate the starting point of each event but rather the centroid of the resonator. This centroid corresponds to the weighted geometric center of the resonant volume, with weights being defined by the distribution of elementary forces during seismic radiation on the limits of that resonator. If this distribution was identical from one event to another, all moment centroids would collapse to a unique point. The spatial extent of the relocated sources gives a minimum volume for the resonant source rather than its total extent.

[39] Deep LPs are characterized by a weak higher-frequency onset followed by a low-frequency wave train (Figure 11). Time delays computed from the entire waveforms lead to alignment of the most energetic and low-frequency parts of the waveforms. This leads, however, to misalignments of the higher-frequency onsets (Figure 11). This observation tends to confirm the trigger/resonator hypothesis and suggests that the trigger may be dissociated from the resonator and its relative position to the resonator may be changing. Sources of these relatively high frequency onsets may be fracturing of the rock by the hot and pressurized magma for example. In some cases onsets are similar, but generally they are unclear and different. Then, the similarity of the signals is due to the similarity of the strong amplitude LP wave trains.

[40] Also, for deep LPs, we see a clear discrepancy between the catalog locations obtained when picking the arrival times (beginning of the waveform) and those deduced from the use of amplitudes calculated on long duration windows. Indeed, because amplitudes are mainly calculated on the low-frequency part of the signal, the obtained locations indicate the position of the resonator. In contrast, sources obtained using arrival times may rather indicate the location of the triggers. Such a hypothesis may be supported by the fact that absolute locations seems to surround the deep relocated cluster (Figure 14) which absolute position was determined from amplitude locations. We, however, note that the precision of the locations based on arrival times is generally poor for deep LPs.

[41] There is a remarkable and systematic delay of variable duration between the high-frequency onset of deep LPs and the low-frequency wave train during which there is little seismic radiation. A possible interpretation is that during this delay, whose duration is from 1 to 4 s, stress propagates as a pressure wave along the conduit, without radiating seismic energy. At that depth, gases may be dissolved in the magma, or exist as a gas phase in the case of CO_2 [*Gerlach and Graeber*, 1985], and are able to be elastically compressed. Compressibility of the magma strongly increases with magma volatile content [*Huppert and Woods*, 2002], especially when volatiles exsolve to form bubbles. In favorable conditions, depression due to the pressure wave may induce the exsolution of gases and tends to increase magma compressibility and wave propagation. Eventually, the pressure perturbation reaches a larger magma volume (larger crack or magma chamber) in the plumbing system where it induces a resonant movement of the magma at the origin of the low-frequency part of the LP event. This simple model may explain the variable time delay and the similarity of the LP waveforms as they are generated by the same fluid-filled volume. A possible explanation for the presence of deep LPs with nonsimilar waveforms and issued from the same volume according to amplitude locations may be the multiple activation of the LP source by successive triggers as observed by *Stephens and Chouet* [2001] at Redoubt volcano.

Appendix A: Calibration of the Network

[42] The use of seismic amplitudes requires first to correct for the possible presence of recording site effects. *Koyanagi et al.* [1995] showed that coda amplification factors can be used to smooth the amplitude distributions of *T* phases recorded on the island of Hawaii. *Aki and Ferrazzini* [2000] showed that for most of the seismic events recorded on the Piton de la Fournaise volcano, spatial amplitude distributions, once corrected using coda site amplification factors, are smooth and simple. On the basis of those results we calculated such factors for the stations of the Hawaiian Volcano Observatory monitoring network.

[43] The calculation of those factors is based on the assumption that for local events, the amplitude decay of coda waves is common to all stations of the network. Then, for lapse times greater than twice the S arrival time [*Rautian and Khalturin*, 1978], the spectral ratio of coda, recorded at

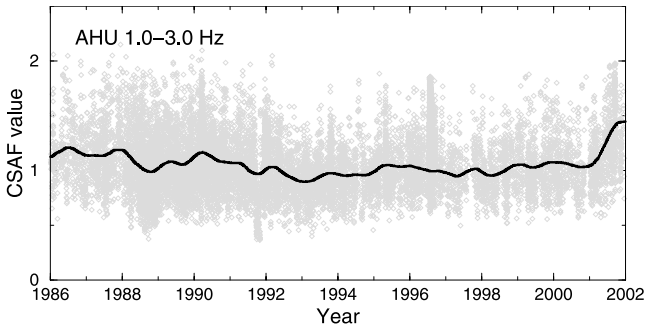

Figure 15. Value of the coda site amplification factor (CSAF) at station AHU and for the frequency band between 1.0 and 3.0 Hz, between 1986 and 2001. The thick black line corresponds to the factor as a function of time obtained after averaging over the individual measurements shown in the background in gray.

two stations and at the same lapse time from the same event, is free of source and path effects and depends only on the local site amplifications at the two stations. Practically, site amplification factors are usually obtained by considering amplitude ratios of coda amplitude (for the same time lapses and same frequency bands) relative to a single station.

[44] For the calculation of the amplification factors we selected local earthquakes with a focal depth greater than 8 km and recorded by at least 20 stations. Amplitudes have been calculated in seven frequency bands, 0.5–1.5, 1.0–3.0, 2.0–4.0, 3.0–5.0, 4.0–6.0, 5.0–10.0, and 10.0–15.0 Hz, using RMS for 10.24 s windows extracted after twice the arrival time of S waves. Amplitudes have been calculated after correcting for the instrument response of the acquisition chain (seismometer, amplifier, VCO, discriminator and digitizer) and amplitudes lower than twice the amplitude of the background noise, estimated over a window selected prior to the onset of each earthquake, have been rejected. For each event, frequency band and coda window, we used as a reference the mean amplitude calculated over measurements coming from at least 15 stations. We noticed that ratios obtained this way were usually more stable than those calculated using a single reference station. However, we also noticed a great variability of the site amplification factors, depending on the coda window for a given event, but also depending on the location of the event as well as on the period of study for a given station. The dependence on the coda window may be related to the fact that we have to choose our signal windows in the early part of the coda because of the limited duration of the available triggered recordings. Early past twice the arrival time of S waves, the common decay assumption may still be perturbed by the presence of source and path effects [*Got and Coutant*, 1997]. Further work is needed to investigate the signification of the coda ratio variability, especially concerning the time and origin dependence [*Aki and Ferrazzini*, 2000].

[45] Because of the great variability of the coda amplitude ratios, ratios have been calculated for about 14000 events (i.e., between 500 and 1500 events per year depending on the available data) selected during the complete period from 1986 to the end of 2001. The final coda site amplification factors have been obtained as a function of time (one value per day) after averaging over a very large number of ratios. The values obtained this way are sufficiently stable for properly correcting for recording site effects. Figure 15 shows the example of the time dependent amplification factor computed at station AHU for the frequency band from 1.0 to 3.0 Hz.

[46] **Acknowledgments.** We are grateful to the members of the Hawaiian Volcano Observatory seismic team for providing high-quality seismic data. Constructive reviews by David Hill and an anonymous reviewer as well as comments from the Associate Editor Joan Gomberg helped improving the quality of this manuscript. We thank the Center for the Study of Active Volcanoes for providing financial support for this work.

References

Aki, K., and V. Ferrazzini, Seismic monitoring and modeling of an active volcano for prediction, *J. Geophys. Res.*, *105*, 16,617–16,640, 2000.

Aki, K., M. Fehler, and S. Das, Source mechanism of volcanic tremor: Fluid driven crack models and their application to the 1963 Kilauea eruption, *J. Volcanol. Geotherm. Res.*, *2*, 259–287, 1977.

Almendros, J., B. Chouet, and P. Dawson, Spatial extent of a hydrothermal system at Kilauea Volcano, Hawaii, determined from array analyses of shallow long-period seismicity: 1. Method, *J. Geophys. Res.*, *106*, 13,565–13,580, 2001a.

Almendros, J., B. Chouet, and P. Dawson, Spatial extent of a hydrothermal system at Kilauea Volcano, Hawaii, determined from array analyses of shallow long-period seismicity: 2. Results, *J. Geophys. Res.*, *106*, 13,581–13,597, 2001b.

Battaglia, J., and K. Aki, Location of seismic events and eruptive fissures on the Piton de la Fournaise volcano using seismic amplitudes, *J. Geophys. Res.*, *108*(B8), 2364, doi:10.1029/2002JB002193, 2003.

Caplan-Auerbach, J., T. Petersen, and S. R. McNutt, Unusual Hybrid Earthquakes at Shishaldin Volcano, Alaska, *Eos Trans. AGU*, *83*(47), Fall Meet. Suppl., Abstract V21A-1172, 2002.

Chouet, B., Ground motion in the near field of a fluid-driven crack and its interpretation in the study of volcanic tremor, *J. Geophys. Res.*, *86*, 5985–6016, 1981.

Chouet, B., Excitation of a magma buried pipe: A seismic source model for volcanic tremor, *J. Geophys. Res.*, *90*, 1881–1893, 1985.

Chouet, B., Long-period volcano seismicity: Its source and its use in eruption forecasting, *Nature*, *380*, 309–316, 1996.

Chouet, B., R. A. Page, C. D. Stephens, J. C. Lahr, and J. A. Power, Precursory swarms of long-period events at redoubt volcano (1989–1990), Alaska: Their origin and use as a forecasting tool, *J. Volcanol. Geotherm. Res.*, *62*, 95–135, 1994.

Clague, D. A., and G. B. Dalrymple, The Hawaiian-Emperor volcanic chain, part I, geologic evolution, *U.S. Geol. Surv. Prof. Pap.*, *1350*, 5–54, 1987.

Crosson, R. S., and D. A. Bame, A spherical source model for low-frequency volcanic earthquakes, *J. Geophys. Res.*, *90*, 10,237–10,247, 1985.

Decker, R. W., Dynamics of Hawaiian volcanoes: An overview, *U.S. Geol. Surv. Prof. Pap.*, *1350*, 997–1018, 1987.

Delaney, P. T., R. S. Fiske, A. Miklius, A. T. Okamura, and M. Sako, Deep magma body beneath the summit and rift zones of Kilauea Volcano, Hawaii, *Science*, *247*, 1265–1372, 1990.

Eaton, J. P., and K. J. Murata, How volcanoes grow, *Science*, *132*, 925–938, 1960.

Falsaperla, S., E. Privitera, B. Chouet, and P. Dawson, Analysis of long-period events recorded at Mount Etna (Italy) in 1992 and their relationship to eruptive activity, *J. Volcanol. Geotherm. Res.*, *114*, 419–440, 2002.

Ferrick, M. G., A. Qamar, and W. F. St. Lawrence, Source mechanism of volcanic tremor, *J. Geophys. Res.*, *87*, 8675–8683, 1982.

Frémont, M.-J., and S. D. Malone, High precision relative locations of earthquakes at Mount St. Helens, Washington, *J. Geophys. Res.*, *92*, 10,223–10,236, 1987.

Gerlach, T. M., and E. J. Graeber, Volatile budget at Kilauea Volcano, *Nature*, *313*, 273–277, 1985.

Gillard, D., A. M. Rubin, and P. Okubo, Highly concentrated seismicity caused by deformation of Kilauea's deep magma system, *Nature*, *384*, 343–346, 1996.

Got, J.-L., and O. Coutant, Anisotropic scattering and travel time delay analysis in Kilauea Volcano, Hawaii, earthquake coda waves, *J. Geophys. Res.*, *102*, 8397–8410, 1997.

Got, J.-L., and P. Okubo, New insights into Kilauea's volcano dynamics brought by large-scale relative relocation of microearthquakes, *J. Geophys. Res.*, *108*(B7), 2337, doi:10.1029/2002JB002060, 2003.

Got, J.-L., J. Fréchet, and F. W. Klein, Deep fault plane geometry inferred from multiplet relative relocation beneath the south flank of Kilauea, *J. Geophys. Res.*, *99*, 15,375–15,386, 1994.

Huppert, E. H., and A. W. Woods, The role of volatiles in magma chamber dynamics, *Nature*, *420*, 493–495, 2002.

Jenkins, G. M., and D. G. Watts, *Spectral Analysis and Its Applications*, Holden-Day, Boca Raton, Fla., 1968.

Julian, B. R., Volcanic tremor: Nonlinear excitation by fluid flow, *J. Geophys. Res.*, *99*, 11,859–11,877, 1994.

Klein, F. W., R. Y. Koyanagi, J. S. Nakata, and W. R. Tanigawa, The seismicity of Kilauea's magma system, *U.S. Geol. Surv. Prof. Pap.*, *1350*, 1019–1185, 1987.

Koyanagi, R. Y., B. Chouet, and K. Aki, Origin of volcanic tremor in Hawaii, part 1, *U.S. Geol. Surv. Prof. Pap.*, *1350*, 1221–1257, 1987.

Koyanagi, S., K. Mayeda, and K. Aki, Frequency dependent site amplification factors using the *S*-wave coda for the island of Hawaii, *Bull. Seismol. Soc. Am.*, *82*, 1151–1185, 1992.

Koyanagi, S., K. Aki, N. Biswas, and K. Mayeda, Inferred attenuation from site effect-corrected *T* phases recorded on the island of Hawaii, *Pure Appl. Geophys.*, *144*, 1–17, 1995.

Kubotera, A., Volcanic tremor at Aso volcano, in *Physical Volcanology*, edited by L. Civetta et al., pp. 29–48, Elsevier Sci., New York, 1974.

Lockwood, J. C., R. Tilling, R. Holcomb, F. Klein, A. Okamura, and D. Peterson, Magma migration and resupply during the 1974 eruptions of Kilauea Volcano, Hawaii, *U.S. Geol. Surv. Prof. Pap.*, *1613*, 1999.

Minakami, T., Seismology of volcanoes in Japan, in *Physical Seismology*, edited by L. Civetta et al., pp. 1–27, Elsevier Sci., New York, 1974.

Poupinet, G., W. L. Ellsworth, and J. Fréchet, Monitoring velocity variations in the crust using earthquakes doublets: An application to the Calaveras fault, California, *J. Geophys. Res.*, *89*, 5719–5731, 1984.

Rautian, T. G., and V. I. Khalturin, The use of the coda for determination of the earthquake source spectrum, *Bull. Seismol. Soc. Am.*, *68*, 923–948, 1978.

Ramos, E. G., M. W. Hamburger, G. L. Pavlis, and E. P. Laguerta, The low-frequency earthquake swarms at Mont Pinatubo, Philippines: Implication for magma dynamics, *J. Volcanol. Geotherm. Res.*, *92*, 295–320, 1999.

Ryan, P. R., R. Y. Koyanagi, and R. S. Fiske, Modeling the three-dimensional structure of macroscopic magma transport systems: Application to Kilauea Volcano, Hawaii, *J. Geophys. Res.*, *86*, 7111–7129, 1981.

Stephens, C. D., and B. A. Chouet, Evolution of the December 14, 1989 precursory long-period event swarm at Redoubt Volcano, Alaska, *J. Volcanol. Geotherm. Res.*, *109*, 133–148, 1989.

St. Lawrence, W., and A. Qamar, Hydraulic transients: A seismic source in volcanoes and glaciers, *Science*, *203*, 654–656, 1979.

Swanson, D. A., W. A. Duffield, D. B. Jackson, and D. W. Peterson, Chronological narrative of the 1969–71 Mauna Ulu eruption of Kilauea Volcano, Hawaii, *U.S. Geol. Surv. Prof. Pap.*, *1056*, 1979.

Tilling, R. I., Fluctuations in surface height of active lava lakes during the 1972–1974 Mauna Ulu eruption of Kilauea Volcano, Hawaii, *J. Geophys. Res.*, *92*, 13,721–13,730, 1987.

Tilling, R. I., and J. Dvorak, Anatomy of a basaltic volcano, *Nature*, *363*, 125–133, 1993.

Wilson, J. T., Evidence from islands on the spreading of the sea floor, *Nature*, *197*, 536–538, 1963.

Wolfe, C. J., P. G. Okubo, and P. M. Shearer, Mantle fault zone beneath Kilauea Volcano, Hawaii, *Science*, *300*, 478–480, 2003.

Wolfe, E. W., (Ed.), The Puu Oo eruption of Kilauea Volcano, Hawaii: Episodes 1 through 20, January 3, 1983, through June 8, 1984, *U.S. Geol. Surv. Prof. Pap.*, *1463*, 1988.

J. Battaglia, Department of Geology and Geophysics, University of Wisconsin-Madison, 1215 W. Dayton St., Madison, WI 53706, USA. (battag@geology.wisc.edu)

J.-L. Got, LGIT, Université de Savoie, Le Bourget du Lac, F-73376, France. (jean-luc.got@univ-savoie.fr)

P. Okubo, U.S. Geological Survey, Hawaii Volcano Observatory, P.O. Box 51, Hawaii National Park, HI 96718, USA. (pokubo@usgs.gov)